Multi-Scale Modeling in Rodent Ventricular Myocytes: Contributions of structural and functional heterogeneities to excitation-contraction coupling

Shaoying Lu[1,2,7], Anushka Michailova[1], Jeffrey Saucerman[1,8], Yuhui Cheng[3], Zeyun Yu[2], Timothy Kaiser[4], Wilfred Li[4], Randolph E. Bank[2], Michael Holst[2], J. Andrew McCammon[3], Takeharu Hayashi[5], Masahiko Hoshijima[6], Peter Arzberger[4] and Andrew D. McCulloch[1]

[1]Department of Bioengineering, UCSD, La Jolla, CA
[2]Department of Mathematics, UCSD, La Jolla, CA
[3]Department of Chemistry and Biochemistry, Department of Pharmacology, Howard Hughes Medical Institute, UCSD, La Jolla, CA
[4]National Biomedical Computation Resource, UCSD, La Jolla, CA
[5]National Center for Microscopic and Imaging Research, UCSD, CA
[6]Department of Medicine, UCSD, La Jolla, CA
[7]Department of Bioengineering, University of Illinois, Urbana-Champaign, IL
[8]Department of Biomedical Engineering, University of Virginia, VA

Running title: Modeling excitation-contraction coupling in ventricular myocytes

Keywords: ventricular myocytes, excitation-contraction coupling, ion channel distribution, reaction diffusion equations, finite element method

Address for correspondence:
Anushka Michailova, Ph.D.
Department of Bioengineering, PFBH 241
University of California San Diego
9500 Gilman Drive, La Jolla, CA 92093-0412
Phone: 858 822 4872
Fax: 858 534 5722
E-mail: *amihaylo@bioeng.ucsd.edu*

Introduction

There is a growing body of experimental evidence suggesting that the Ca^{2+} signaling in ventricular myocytes is characterized by high gradient near the cell membrane and a more uniform Ca^{2+} distribution in the cell interior [1]-[7]. An important reason for this phenomenon might be that in these cells the t-tubular system forms a network of extracellular space, extending deep into the cell interior. This allows the electrical signal, that propagates rapidly along the cell membrane, to reach the vicinity of the sarcoplasmic reticulum (SR) where intracellular Ca^{2+} required for myofilament activation is stored [1], [8]-[11]. Early studies of cardiac muscle showed that the t-tubules are found at intervals of ~2 μm along the longitudinal cell axis in close proximity to the Z-disks of the sarcomeres [12]. Subsequent studies have demonstrated that the t-tubular system has also longitudinal extensions [9]-[11], [13].

The SR is an entirely intracellular, membrane-bounded compartment that abuts but is not continuous with the sarcolemma. The junctions where SR approaches the sarcolemma contain specialized proteins [1], [4], [14]. The sarcolemmal L-type Ca^{2+} channels (LCC) are located primarily at the SR junctions where the Ca^{2+} release channels in the SR, the ryanodine receptors (RyRs), exist [2], [3], [11], [15]-[17]. The RyRs are arranged in organized arrays of hundreds of receptors up to 200 nm in diameter.

The concept that the LCCs and RyRs form a local functional unit (release unit, RU) is supported by the observations of Ca^{2+} sparks. Ca^{2+} sparks reflect the nearly synchronous activation of a cluster of about 6-20 RyRs at a single junction. Ca^{2+} sparks are the fundamental units of the SR Ca^{2+} release both at rest and during cell excitation [1], [3]-[7]. Thus, the microanatomy of t-tubules and SR permits spatially homogeneous

and synchronized SR Ca^{2+} release throughout the cell. During physiologically normal excitation-contraction coupling (EC-coupling) a several thousand Ca^{2+} sparks in each cell are synchronized in time by the action potential to achieve a spatially homogeneous Ca^{2+} transient [1], [4]-[6], [8], [14]. It has also been observed that the spatially uniform Ca^{2+} transient might be achieved if the SR Ca^{2+} release and uptake are abolished [8]. However the mechanisms underlying cell activation synchrony and Ca^{2+} homogeneous distribution still remains unclear.

Recent immunohistochemical studies but one [17] have demonstrated also that marked variations in the distribution of Ca^{2+}-handling proteins (L-type Ca^{2+} channel, Na^+/Ca^{2+} exchanger, sarcolemmal Ca^{2+} ATPase) along the cell membrane probably exist [10], [11], [15], [16]. The analysis suggests that most of the L-type Ca^{2+} channels are concentrated in the t-tubules (from 3 to 9 times more in the t-tubule membrane than on the surface sarcolemma) and that the concentration of LCC along the t-tubule increases toward the center of the cell [10], [16].

Studies on the distribution of the main Ca^{2+} efflux pathway, the Na^+/Ca^{2+} exchanger (NCX), are more controversial. All studies but one [18] have reported NCX to localize both to the surface and t-tubule membrane, and most studies suggest that the NCX is 1.7 to 3.5 times more concentrated in the t-tubule membrane, [15], [18]-[20]. However, Kieval *et al*. data [21] indicate the NCX is more evenly distributed. The distribution of the sarcolemmal Ca^{2+} ATPase is also unclear [10]. Only one study reports that in hamster and canine ventricular cells this Ca^{2+} efflux pathway is located predominantly in the surface membrane [22]. In summary, the observed differences in the spatial distribution and molecular architecture of Ca^{2+} microdomains suggest that

significant differences in the EC-coupling between the cell surface and cell interior may exist. However how the localization of Ca^{2+}-handling proteins along the sarcolemma regulates the intracellular Ca^{2+} signaling still remains uncertain.

Taken together above studies demonstrate that remarkable amount of fundamental quantitative data on the ventricular cell structure and function has been accumulated. Recently it has been also emphasized that biophysically realistic computational models, incorporating transverse-axial t-tubular system and considering geometric irregularities and inhomogeneities in the distribution of ion-transporting proteins, are missing and needed [11], [23]. For this reason, our main goal here was to develop a detailed 3-D model at the sub-cellular level that would allow us to examine how the distribution of Ca^{2+} fluxes via t-tubule and surface membrane may affect Ca^{2+}-entry, diffusion and buffering. Thus, SR Ca^{2+} uptake and release was not included here. The current model of the rat ventricular myocyte includes: (1) a simplified 3-D geometry of a single t-tubule and its surrounding half-sarcomeres; (2) the spatially distributed L-type Ca^{2+} channel, Na^+/Ca^{2+} exchanger, sarcolemmal Ca^{2+} pump and background Ca^{2+} leak along the sarcolemma; and (3) the stationary and mobile endogenous Ca^{2+} buffers (troponin C, ATP, calmodulin) and the exogenous mobile Ca^{2+} buffer, Fluo-3.

The results suggest that, in the presence of 100 µM Fluo-3, the model is able to predict a uniform Ca^{2+} distribution inside the cell if Ca^{2+} microdomains are distributed heterogeneously along the cell membrane. In the absence of Ca^{2+} indicator the model predicts non-uniform Ca^{2+} distribution in the cytoplasm and high Ca^{2+} gradient near the cell edges when the Ca^{2+} flux pathways were distributed heterogeneously. We concluded that the distribution of Ca^{2+} handling proteins along the cell membrane might be another

4

important mechanism regulating ventricular EC-coupling. These model predictions are in qualitative agreement with published experimental data in rat ventricular myocytes [8]. Preliminary results of this work have been presented to the Biophysical Society in abstract form [24].

It is important to mention here that this 3-D sub-cellular model of single t-tubule and surrounding structures also yields insights across two other scales of biological organization: a microscopic scale of individual Ca^{2+} RU and a whole-cell scale. It allows us not only to extend the analysis further to integrate models of individual Ca^{2+} RU, SR Ca^{2+} pump or leak but also to examine how experimentally suggested spatial distributions of these Ca^{2+} transporters [2], [3], [11], [15]-[17] may affect the behavior of a single RU or the mechanisms underling a synchronized SR Ca^{2+} release. Future modeling efforts will be focused on replacing the idealistic t-tubule and surrounding structures geometries with more realistic or to include several surrounding t-tubules and other sub-cellular organelles that might help to understand better normal and pathophysiological mechanisms.

Materials and Methods

Model cell geometry and spatial protein distribution along the cell membrane

The model geometry was derived from the published structural data [9], [11], [23]. The cell model contains one repeating unit inside the ventricular myocyte, including single t-tubule and its surrounding half-sarcomeres (Fig. 1A and Table 1). The t-tubule was assumed to be cylinder, with a diameter of 0.25 μm and a depth of 6.87 μm. The surrounding half-sarcomeres were modeled as a cube-shaped box enclosing the t-tubule

5

with dimensions 2 μm ×2 μm in the plane of the cell surface and 7 μm in depth. The volume of the model compartment was estimated to be ~27.68 μm^3. The compartment membrane area was ~9.34μm^2 where the percentage of cell membrane within t-tubule was 58% (~5.42 μm^2) and within the surface membrane 42% (~3.92 μm^2), [9], [11], [23], [25].

Figure 1A-B and Table 1 - near here

The accessible volume for Ca^{2+} was estimated from reported measurements in adult rat ventricular myocytes [1], [26]. These data, suggest that myofilaments occupy 47-48 % of the cell volume, mitochondria 34-36%, nucleus 0-2%, t-tubule system 0-1.2% and SR lumen 3.5%. The experiments also suggest that about 50% of the myofilament space is accessible for Ca^{2+} ions (i.e. contains water) and that mitochondria and nuclei are not rapidly accessible for Ca^{2+} [1], [27]. In this study we also assume that the SR lumen is not accessible to Ca^{2+} in the presence of ryanodine and thapsigargin. Thus, from the experimental data and above assumptions, the accessible volume for Ca^{2+} in adult rat ventricular cells was estimated to be ~35-37% of the total cytosolic volume (V_{acc}) ~12.9-13.6 pL.

The depth of the cleft between the sarcolemmal and SR membranes, where the LCC and RyR localize, has been reported to be 12-20 nm [27] and the sub-sarcolemma space between cellular membrane and myofibrils ~45 nm [1]. In this study, the size of both spaces was considered infinitely thin on the scale of the continuum model. This assumption allowed: (1) not to explicitly define a different diffusion coefficients for Ca^{2+} and mobile buffers (Fluo-3, ATP, Cal) in the cleft, sub-sarcolemmal and myofibril spaces

6

as in Michailova *et al.* [27], (2) to simplify the model and to improve the model stability and efficiency.

In agreement with reported experimental data, Ca^{2+} transporters were distributed heterogeneously along the model cell surface (Fig. 1B and 2A). The concentration of LCC in the t-tubule membrane was 6 times of that in the surface membrane and increased 1.7-fold along the length of the t-tubule. The concentration of NCX in the t-tubule membrane was three times that in the surface membrane. The sarcolemmal Ca^{2+} ATPase was located only in the surface membrane. The background Ca^{2+} leak was assumed to be present throughout the whole sarcolemma because no data were available of how this Ca^{2+} channel is distributed.

In the axial t-tubule direction, the distribution of LCC current was computed by combining the cluster density and fluorescent intensity plots [16]. The data were then scaled and fitted by a cubic polynomial:

$$f(x) = p_1 x^3 + p_2 x^2 + p_3 x + p_4 \tag{1}$$

where: x is the distance from the cell surface.

The parameter values of the polynomial (p_j, j=1-4) are shown in Table 2. This polynomial was further scaled by a single factor C (see Table 2) such that the total Ca^{2+} flux along the t-tubule membrane remained unchanged by redistributing the Ca^{2+} fluxes.

Figure 2A-B and Table 2 - near here

Reaction-diffusion equations

The effects of four exogenous and endogenous Ca^{2+} buffers (Fluo-3, ATP, calmodulin, troponin C) were considered (Fig. 1B). The endogenous stationary buffer troponin C (TN) was distributed uniformly throughout the cytosol but not on the cell membrane. The

free Ca^{2+} and mobile buffers (Fluo-3, ATP, calmodulin) diffuse and react throughout the cytoplasm and cell membrane subject to reflective boundary conditions at the cell surfaces. The nonlinear reaction-diffusion equations describing Ca^{2+} and buffers dynamics inside the cell are:

$$\frac{\partial [Ca^{2+}]_i}{\partial t} = D_{Ca} \nabla^2 [Ca^{2+}]_i - \sum_{m=1}^{3} R_{B_m} - R_{B_s} + J_{Ca_{flux}} \qquad (2)$$

$$\frac{\partial [CaB_m]}{\partial t} = D_{CaB_m} \nabla^2 [CaB_m] + R_{B_m} \qquad (3)$$

$$\frac{\partial [CaB_s]}{\partial t} = R_{B_s} \qquad (4)$$

$$R_{B_m} = k_+^m ([B_m] - [CaB_m])[Ca^{2+}]_i - k_-^m [CaB_m] \qquad (5)$$

$$R_{B_s} = k_+^s ([B_s] - [CaB_s])[Ca^{2+}]_i - k_-^s [CaB_s] \qquad (6)$$

where: $[B_m]$ mobile buffer Fluo-3, calmodulin or ATP; $[B_s]$ stationary buffer troponin C.

The diffusion coefficients for Ca^{2+}, CaATP, CaCal and CaFluo as well as the total buffer concentrations and rate buffer constants used in the model are shown in Table 3. In the model we also assume: (1) Ca^{2+} binds to Fluo-3, calmodulin, ATP, and TN without cooperativity; (2) the initial total concentrations of the mobile buffers are spatially uniform; (3) the diffusion coefficients of Fluo-3, ATP or calmodulin with bound Ca^{2+} are equal to the diffusion coefficients of free Fluo-3, ATP or calmodulin.

Table 3 - near here

The total Ca^{2+} flux ($J_{Ca_{flux}}$) throughout the t-tubule and surface membrane is:

$$J_{Ca_{flux}} = J_{Ca} - J_{NCX} - J_{pCa} + J_{Cab} \qquad (7)$$

8

where: J_{Ca} - total LCC Ca^{2+} influx; J_{NCX} - total NCX Ca^{2+} efflux; J_{pCa} - total Ca^{2+} pump efflux; J_{Cab} - total background Ca^{2+} leak influx.

To fit the whole-cell LCC current density to reported data in rat myocytes with SR release inhibited [28] we used a MATLAB implementation of Hinch *et al.* model [29], (Fig. 2B). To describe the Na$^+$/Ca^{2+} exchanger, membrane Ca^{2+} pump and leak current densities we used expressions from Hinch *et al.*:

$$I_{NCX} = g_{NCX} \frac{e^{\eta VF/RT}[Na^+]_i^3[Ca^{2+}]_e - e^{(\eta-1)VF/RT}[Na^+]_e^3[Ca^{2+}]_i}{(k_{m,Na}^3 + [Na^+]_e^3)(k_{m,Ca} + [Ca^{2+}]_e)(1 + k_{sat}e^{(\eta-1)VF/RT})} \qquad (8)$$

$$I_{pCa} = \frac{g_{pCa}[Ca^{2+}]_i}{[Ca^{2+}]_i + k_{m,pCa}} \qquad (9)$$

$$I_{Cab} = g_{Cab}\left[\frac{RT}{2F}\ln\left(\frac{[Ca^{2+}]_e}{[Ca^{2+}]_i}\right) - V\right] \qquad (10)$$

Flux parameter values were estimated or taken from the literature (see Table 4). At rest the Ca^{2+} influx via background Ca^{2+} leak was adjusted to match the Ca^{2+} efflux via NCX and Ca^{2+} ATPase so that no net movement across the cell membrane occurred.

Table 4 - near here

In the model, each current density (I_i) was converted to Ca^{2+} flux (J_i) by using the experimentally suggested surface to volume ratio ($\frac{C_m}{V_{cell}} \sim$ 8.8 pF/pL) in adult rat ventricular myocytes [1], [25]:

$$J_i = \left(\frac{1}{2F}\frac{C_m}{V_{cell}}\right)I_i \qquad (11)$$

Then, the total compartment Ca^{2+} flux ($J_{Ca_{flux}}$) was computed by multiplying each total J_i with the model cell volume (V_{mc}), and distributing $J_{Ca_{flux}}$ to the surface membrane and t-tubule membrane according to the prescribed Ca^{2+} handling protein concentration ratio.

Software

The nonlinear reaction diffusion system was solved using a finite difference method in time and finite element method in space. Here we developed a distributed finite element software package, to be used on a Linux cluster for parallel computations. Computations took ~18 minutes to simulate 400 ms of one Ca^{2+} cycle on 10 processors of an Intel Xeon-based cluster (see Fig 3B). A discrete time stepping of 4ms was used during the simulations.

The software was built using several established software packages. Mesh generators included Netgen4.3.1 and TetGen1.3 authored by Schöberl and Si respectively [30]. The parallel finite element assembler was based on libMesh0.4.3-rc2 by Kirk *et al.* [31]. The discrete linear system was solved using PETSc-2.2.1 [32]. An operator splitting method was used to de-couple the reaction-diffusion system [33]. The nonlinear ordinary differential equations were solved using an A-stable and implicit Runge-Kutta method of order 5. The simulation results were visualized using GMV3.4 [34]. Post-processing and data analysis were performed using customized Python and MATLAB version 7.1 (The MathWorks, Natick, MA) scripts.

In designing the software, the portability and reusability were emphasized over computational efficiency. The implementation was based on object-oriented programming. Therefore the resulting software contains a set of loosely connected

application tools, which focused on both flexibility and functionality. The structure of the software followed that of a finite element simulation package (Fig. 3A).

Figure 3A-B – near here

Results

Ca²⁺ concentration changes in the presence of 100 μM Fluo-3 and inhibited SR release and uptake

Model results in Fig. 4 were computed for conditions approximating those of experiments by Cheng *et al.* [8] (see Fig. 4M), who examined Ca^{2+} signals in rat ventricular myocytes in the presence of 100 μM Fluo-3 and pharmacological blockade of the SR. The voltage-clamp protocol (holding potential –50mV, electric pulse of 10mV for 70ms) and whole-cell L-type Ca^{2+} current were derived from the study of Zahradnikova *et al*. [28] with blocked SR (see Fig.2B and Figs. 4A-B).

Figure 4A-M - near here

Consistent with the experimental study [8] in the model the scanned line was located at 200nm from the surface of the t-tubule (*see red line* in Fig. 5A). The line-scan images and local Ca^{2+} time-courses are shown in Figs. 4G-I and Figs. 4J-L, respectively. These results suggest that the model was able to predict uniform Ca^{2+} distribution inside the cell when LCC and NCX current densities were heterogeneously and Ca^{2+} leak homogeneously distributed along the sarcolemma and Ca^{2+} pump was located on the surface membrane. Furthermore, when the LCC flux density was 6 times higher and uniform in the t-tubule, the Ca^{2+} concentration profiles were less evenly distributed (Figs. 4H and 4K) but the predicted variations in $[Ca^{2+}]_i$ seem to be within the range of

experimental noise in Fig. 4M. Finally, these studies revealed that heterogeneous Ca^{2+} transients might occur if the LCC current density was uniformly distributed throughout the whole cell surface (Figs. 4I and 4L). The model also demonstrated that distributing NCX flux homogeneously along the sarcolemma did not significantly affect Ca^{2+} uniformity (*data not shown*). The distribution of Ca^{2+} pump and leak pathways also did not seem to have a significant effect. Blockade of these fluxes reduced the control $[Ca^{2+}]_i$ peak in Fig. 4J by less than 0.4% (*data not shown*). Figures 4F and 4C-E show the global $[Ca^{2+}]_i$ transient, Na^+/Ca^{2+} exchanger, Ca^{2+} pump and leak currents when Ca^{2+} pathways were distributed heterogeneously as in Fig. 4G. Figures 4F and 4J-L illustrate: (1) that the global and all local Ca^{2+} transients reached the peak after ~ 68 ms; and (2) that the decay of the Ca^{2+} signals was extremely slow, since the reuptake of Ca^{2+} to the SR was blocked and $[Ca^{2+}]_i$ was lowered solely by extrusion from the cell via the Na^+-Ca^{2+} exchanger and Ca^{2+} pump. Possible reasons for the predicted extremely slow NCX rate might be that in the model the intracellular Na^+ concentration ($[Na^+]_i$) was kept constant (in contrast to existing evidence for the presence of local sub-membrane $[Na^+]_i$ gradients on the action potential time-scale [1], [35]) or that the realistic distribution of NCX flux density probably differs as assumed in the model. The 3-D Ca^{2+} concentration distributions at Ca^{2+} peak (line scan 200 nm away from the t-tubule) and the local Ca^{2+} transients (line scan 0 nm and 875 nm away from the t-tubule) are shown in Fig. 5.

Figure 5A-G - near here

In summary, the results in Fig. 4 and Fig. 5 suggest that in the presence of 100 μM Fluo-3 and with the SR blocked (1) Ca^{2+} concentration near the surface membrane decreased while $[Ca^{2+}]_i$ in the cell interior increased when Ca^{2+} transporters were

12

uniformly distributed and after that heterogeneously redistributed, and (2) in each moment of the cell cycle the overall Ca^{2+} distribution remained almost uniform across the model compartment when Ca^{2+} transporters were heterogeneously distributed.

The good agreement between the model and experimental observations suggests that heterogeneous channel distributions may be another important mechanism regulating intracellular Ca^{2+} distribution and myofilament function. Moreover, it allows the model to be used to simulate experiments that cannot be performed because of technical reasons (for example in the absence of Ca^{2+} indicator).

Ca^{2+} concentration changes in the absence of Fluo-3, inhibited SR and heterogeneous distribution of Ca^{2+} membrane pathways

Figure 6 shows membrane currents, and Ca^{2+} signals arising from the ionic influx via L-type Ca^{2+} channels at zero Fluo-3 with heterogeneously distributed membrane Ca^{2+} fluxes (as in Fig. 4G) during voltage-clamp stimulation.

<center>**Figure 6A-J - near here**</center>

Since it has been suggested [2], [36] that the dye does not affect Ca^{2+} entry via L-type channels, the same global LCC flux was used during this numerical experiment (Fig. 4B and Fig. 6B). In the absence of Fluo-3 the peak of average Ca^{2+} transient increased ~1.6-fold (from 0.19 µM up to 0.3 µM), while the time to peak (~ 68 ms) remained unchanged (Fig. 6). Figures 6H and 6I-J demonstrate that local Ca^{2+} peaks also increased while the times to peak remained ~ 68 ms. In addition, $[Ca^{2+}]_i$ decay at zero Fluo-3 was slow. The increase in local Ca^{2+} levels across the cell membrane affected Na^{2+}/Ca^{2+} exchange and Ca^{2+} pump activities more significantly than the Ca^{2+} background leak (see Figs. 6C-E and Figs. 4C-E). It is interesting that, under these conditions, the model predicts non-

<center>13</center>

uniform Ca^{2+} concentration distributions in and along the cell membrane and in the cell interior. Figures 6 I-K demonstrate that in the absence of Fluo-3 $[Ca^{2+}]_i$ in and near the t-tubule membrane was much more higher than in the cell interior. These results indicate that Ca^{2+} levels vary in the transverse direction too. Along the t-tubule, $[Ca^{2+}]_i$ was higher near to the surface membrane and in the cytoplasmic t-tubule end while in the cell interior $[Ca^{2+}]_i$ was higher only near the surface membrane.

Discussion

In this study we developed a 3-D continuum model of Ca^{2+}-signaling, buffering and diffusion inside a small representative region of the rat ventricular muscle cell. The simplified model geometry, derived from published structural data [9], [11], [23], contained one repeating unit inside the myocyte, including single cylindrical t-tubule and its surrounding half-sarcomeres. Following the morphological studies on 3-D reconstruction of t-tubule system, ~58% of membrane surface was assumed to be within the t-tubule. On the basis of experimental data in rat myocytes [26] the aqueous sub-cellular volume, accessible to Ca^{2+}, was estimated to be ~ 35-37%. In addition, we assumed the cleft and sub-membrane sizes infinitely thin that allowed us not to explicitly define a deferent values for D_{Ca}, D_{CaFluo}, D_{CaATP} and D_{CaCal} in these near-membrane spaces and in myofibrils. To test the correctness of above assumption we examined how 2-fold increase in D_{Ca} or mobile buffer diffusion coefficients (values suggested in water) in the cleft and sub-membrane space or variations in the sub-membrane depth (from 12 nm to 45 nm) would affect local and global Ca^{2+} transients. We found that these changes had insignificant effects on the calculated Ca^{2+} signals (*data not shown*). We concluded

14

that a functional importance of these spaces lies in the immediate vicinity of the sarcolemma where all membrane proteins and sarcolemmal ion channels are located [1-7], [27]. In view of the fact that Ca^{2+} signaling in cells is largely governed by Ca^{2+} diffusion and binding to mobile and stationary Ca^{2+} buffers [3], [27], [37] the effect of four Ca^{2+} buffers (Fluo-3, ATP, calmodulin, TN) was considered. We validated the model against published experimental data on Ca^{2+} influx, membrane protein distributions and Ca^{2+} diffusion in rat ventricular myocytes treated with ryanodine and thapsigargin [8], [10], [15], [16], [18]-[22]. We used the model: (1) to examine how the distribution of L-type Ca^{2+} channels, Na^{+}/Ca^{2+} exchangers, membrane Ca^{2+} ATPases and membrane leaks regulates the spatio-temporal features of intracellular Ca^{2+} signals in the presence of fluorescent dye; and (2) to simulate and analyze the Ca^{2+} signals that are not accessible experimentally, i.e. in the absence of Ca^{2+} indicator. The parallel numerical software enabled us to solve the reaction-diffusion equations in a reasonable time and to test the model carefully.

An important model limitation is that we simplified the t-tubule and surrounding structures geometries assuming them cylindrical and cube-shaped box, respectively. However, several studies provide evidence that in normal ventricular cells the realistic t-tubule geometry is quite complex (with large local variations in the diameter and transverse-axial anatomies) and that its surrounding structures might form quite arbitrary shapes (see Fig.7) [9], [13], [38]. It has been also observed that in the failing hearts the t-tubules might be aberrantly shaped or dilated [13], [39]. Taken together above data strongly suggest that further extending of the current model toward more realistic geometries is needed. The use of idealistic shapes might change the diffusion distances in

plane and depth directions and consequently the predicted Ca^{2+} distributions.

Figure 7 – near here

Ca^{2+} signals in the presence of 100 μM Fluo-3 and absence of SR activity Cheng *et al*. [8] examined the propagation of EC-coupling in isolated rat ventricular cells by using laser scanning confocal microscope and 100 μM Fluo-3. They found that the depolarization-evoked $[Ca^{2+}]_i$ transients in the presence or absence of SR release and uptake are activated synchronously near the cell surface and in the cell interior and that the time of $[Ca^{2+}]_i$ rise does not depend on whether SR activity is abolished or not. They concluded that the lack of systematic differences in the Ca^{2+} fluorescence signal recorded from either the center or the edge of the cell indicates that sarcolemmal Ca^{2+} and the SR Ca^{2+}-release channels (RyRs) are distributed throughout the heart cell, and that ventricular EC-coupling is not limited by diffusion of the second messenger from the surface of the cell to the center.

In this study, to investigate further the mechanisms underlying EC-coupling propagation in rat ventricular myocytes, we used modeling approach. We examined how the distribution of the sarcolemmal Ca^{2+} influx and efflux transporters regulates Ca^{2+} movement from the cell surface to the cell interior when the SR was blocked. In agreement with experiment [10], [16], we found that in the presence of 100 μM Fluo-3 model predicts a homogenous Ca^{2+} distribution inside the cell if L-type Ca^{2+} current density is ~6 times higher in the t-tubule than in surface membrane and increases ~1.7 fold along the t-tubule length. An interesting model observation was also that the uniform Ca^{2+} distribution might be achieved assuming LCC flux density 6-fold higher and

16

uniform along the t-tubule because the predicted $[Ca^{2+}]_i$ fluctuations here were within the range of experimental noise [8]. New experiments should be performed to test this hypothesis.

In addition, our results revealed that the spatio-temporal features of local Ca^{2+} signals depended on the diffusion distances in the axial and cell surface directions. Thus, when the LCC were distributed uniformly the local Ca^{2+} peak in radial depth (7 μm) decreased from ~0.25 μM to ~0.15 μM while in the other cell directions (1 μm x 1 μm) no significant changes were found. Redistributing the amount of Ca^{2+} pumped via the cell membrane (i.e. increasing LCC current density ~6-fold along the t-tubule) while keeping total Ca^{2+} flux unchanged, lowered Ca^{2+} gradients near the surface membrane and increased Ca^{2+} levels in the cell interior.

Other interesting model findings were that: (1) the global Ca^{2+} time-course and time to $[Ca^{2+}]_i$ peak (~68 ms) do not depend on whether Ca^{2+} flux pathways are distributed homogeneously, uniformly in the t-tubule or heterogeneously (*data not shown*); (2) the changes in the local Ca^{2+} transients near the cell membrane when Ca^{2+} microdomains were distributed differently affected NCX and Ca^{2+} pump time-courses while Ca^{2+} leak current remained unchanged (*data not shown*); and (3) the NCX, Ca^{2+} pump or Ca^{2+} leak redistribution alone were not able to alter significantly the predicted Ca^{2+} uniformity (*data not shown*).

Ca^{2+} signals in the absence of Fluo-3 and SR activity and heterogeneous distribution of Ca^{2+} membrane fluxes Another advantage of the model was its ability to predict Ca^{2+} signals that would occur in the absence of Fluo-3. The model simulations revealed that at zero Fluo-3 and with 260 μM ATP and 24 μM calmodulin as mobile buffers, the Ca^{2+}

distribution in the cell interior would be non-uniform if LCC are distributed heterogeneously (as in Figs. 4G). Note in the absence of 100 μM mobile Fluo-3 a local and global Ca^{2+} peaks increased while the time of Ca^{2+} rise remained almost unchanged. Furthermore, during the Ca^{2+} influx larger, steeper and heterogeneous Ca^{2+} concentration gradients were predicted between the cytosol and sub-membrane space while in the cell interior $[Ca^{2+}]_i$ was more uniformly distributed. In addition, results suggest that the calculated sub-membrane $[Ca^{2+}]_i$ levels were higher: (1) near the t-tubule mouth because a close topological proximity of this membrane to the surface sarcolemma additionally increased the relative amount of Ca^{2+} entering there; (2) near the cytosolic t-tubule end because the LCC flux density was assumed higher. The simulations also showed that removing Fluo-3 affected NCX and Ca^{2+} pump time-courses by increasing local free $[Ca^{2+}]_i$. Thus, these findings clearly reveal that (1) the exogenous Fluo-3 may act as a significant buffer and carrier for Ca^{2+}, and that (2) the use of 100 μM Fluo-3 during the experiment may sensitively alter the realistic Ca^{2+} distribution. However the question arising here is: Based on the model what might be the underlying mechanism(s) for the predicted Ca^{2+} concentrations gradients in the absence of Fluo-3? A reasonable answer is that Ca^{2+} movement and distribution inside the cell also strongly relies on the presence of mobile and stationary Ca^{2+} buffers [27], [37]. Thus now in the absence of Fluo-3 (1) the stationary Ca^{2+} buffer troponin C (TN) imposed stronger diffusion barrier for Ca^{2+} that resulted in larger and steeper Ca^{2+} concentration gradients between the cytosol and narrow sub-membrane space, (2) the buffer capacity and spread of ATP and Cal alone via the t-tubule membrane were not able to mask the assumed heterogeneous Ca^{2+} entering via the sarcolemma, (3) in the cell interior, the overall Ca^{2+} distribution remained almost

uniform in each moment of the cell cycle (because TN, ATP and Cal buffering capacity dominated) and a little beat higher in and near the surface membrane (because [TN] was zero there).

Taken together, our studies suggest that in ventricular myocytes when the SR is pharmacologically inhibited: (1) intracellular Ca^{2+} concentration rapidly increases during Ca^{2+} entrance (0-70 ms) while the decay of $[Ca^{2+}]_i$ is slow; (2) in the absence of fluorescent dye, large Ca^{2+} concentration gradients might develop near the cell membrane; and (3) intracellular Ca^{2+} distribution is tightly regulated by the localization of Ca^{2+} transporter proteins along the sarcolemma and strongly relays on the presence of mobile and stationary Ca^{2+} buffers. These studies also imply that in ventricular cells with intact and functional SR, the Ca^{2+} signal most likely would spread faster along the t-tubule and surface membrane than to the cell interior and that in the absence of Ca^{2+} dye high Ca^{2+} gradients under the surface membrane and more uniform Ca^{2+} distribution in the cell interior might be expected.

Acknowledgments

Grants

References

[1] D.M. Bers, *Excitation-contraction coupling and cardiac contractile force.* Kluwer Academic Press, Dortrecht, Boston, London, 2001.

[2] C. Soeller and M.B. Cannell "Analysis of ryanodine receptor clusters in rat and human cardiac myocytes", *PNAS*, vol. 104 (38), pp.14958-14963, 2007.

[3] L. T. Izu, S. A. Means, J.N. Shadid, Ye Chen-Izu, and C. W. Balke, **"**Interplay of Ryanodine Receptor Distribution and Calcium Dynamics", *Biophys. J.*, vol. 91, pp. 95-112, 2006.

[4] M.J. Berridge, M.D. Bootman, and H.L. Roderick, "Calcium signaling: dynamics, homeostasis and remodeling", *Nat. Rev. Mol. Cell. Biol.*, vol. 4, pp. 517-529, 2003.

[5] E. Niggli, "Ca^{2+} sparks in cardiac muscle: Is there life without them?", *News Physiol. Sci.*, vol. 14, pp. 129-134, 1999.

[6] L.A. Blatter, J. Kockskamper, K.A. Sheehan, A.V. Zima, J. Huser, and S. Lipsius, "Local calcium gradients during excitation-contraction coupling and alternans in atrial myocytes", *J. Physiol.*, vol. 546, pp.19-31, 2003.

[7] E.A. Sobie, K.W. Dilly, J.S. Cruz, W.J. Lederer, and M.S. Jafri, "Termination of cardiac Ca^{2+} sparks: An investigative mathematical model of calcium-induced calcium release", *Biophys. J.*, vol.83, pp.59-78, 2002.

[8] H. Cheng, M.B. Cannell, and W.J. Lederer, "Propagation of excitation-contraction coupling into ventricular myocytes", *Pflugers Arch.*, vol. 428, pp. 415-417, 1994.

[9] C. Soeller and M.B. Cannell "Examination of the transverse tubular system in living cardiac rat myocytes by 2-photon microscopy and digital image – processing techniques", *Circ. Res.*, vol. 84, pp.266-275, 1999.

[10] F. Brette and C. Orchard, "T-tubule function in mammalian cardiac myocytes", *Circ. Res.*, vol. 92, pp.1182-1192, 2003.

[11] M. Pásek, F. Brette, A. Nelson, C. Pearce, A. Qaiser, G. Christe and C.H. Orchard, "Quantification of T-tubule area and protein distribution in rat cardiac ventricular myocytes", *Prog. Biophys. Mol. Biol*., vol. 96, pp. 244-257, 2008.

[12] E. Page and L.P. McCallister, "Quantitative electron microscopic description of heart muscle cells: application to normal, hypertrophied and thyroxin-stimulated hearts", *Am. J. Cardiol.*, vol. 31, pp.172-181, 1973.

[13] M.E. Martone, V.M. Edelman, A. Thor, S.J. Young, S.P. Lamont, J. Ross Jr., and M.H. Ellisman, "Three dimensional analysis of transverse tubules in normal and failing heart: A combined confocal and high voltage electron microscope study", *Microscopy and Microanalysis*, vol. 3 (S2), pp. 231-232, 1997.

[14] D.M. Bers, "Calcium cycling and signaling in cardiac myocytes", *Annu. Rev. Physiol.*, vol. 70, pp. 23-49, 2008.

[15] D.R. Scriven, P. Dan, and E.W. Moore, "Distribution of proteins implicated in excitation-contraction coupling in rat ventricular myocytes", *Biophys. J.*, vol. 79, pp. 2682-2691, 2000.

[16] D.R. Scriven, A. Klimek, K.L. Lee, and E.W. Moore, "The molecular architecture of calcium microdomains in rat cardiomyocytes", *Ann. NY Acad. Sci.*, vol. 976, pp. 488-499, 2002.

[17] D.R. Scriven, A. Klimek, P. Asghari, K. Bellve, and E.W. Moore, "Caveolin-3 is adjacent to a group of extradyadic ryanodine receptors", *Biophys. J.*, vol. 89, pp. 1893-1901, 2005.

[18] Z. Yang, C. Pascarel, D.S. Steele, K. Komukai, F. Brette, and C.H. Orchard, "Na+-Ca2+ exchange activity is localized in the T-tubules of rat ventricular myocytes", *Circ. Res.*, vol. 91(4), pp. 315-22, 2002.

[19] S. Despa, F. Brette, C. H. Orchard, and D. M. Bers, "Na/Ca exchange and Na/K-ATPase function are equally concentrated in transverse tubules of rat ventricular myocytes", *Biophys. J.*, vol. 85(5), pp. 3388-3396, 2003.

[20] M.J. Thomas, I. Sjaastad, K. Andersen, P.J. Helm, J.A. Wasserstrom, O.M. Sejersted, and O.P. Ottersen, "Localization and function of the Na+/Ca2+-exchanger in normal and detubulated rat cardiomyocytes", *J. Mol. Cell. Cardiol.*, vol. 35(11), pp. 1325-1337, 2003.

[21] R.S. Kieval, R.J. Bloch, G.E. Lindenmayer, A. Ambesi, and W.J. Lederer, "Immunofluorescence localization of the Na-Ca exchanger in heart cells", *Am. J. Physiol.*, vol. 263, pp. C545-C550, 1992.

[22] Y. Iwata, H. Hanada, M. Takahashi, and M. Shigekawa,"Ca(2+)-ATPase distributes differently in cardiac sarcolemma than dihydropyridine receptor alpha 1 subunit and Na+/Ca2+ exchanger", *FEBS Lett.*, vol. 355(1), pp. 65-68, 1994.

[23] M. Pásek, J. Šimurda, G. Christé and C.H. Orchard, "Modelling the cardiac transverse-axial tubular system", *Prog. Biophys. Mol. Biol*., vol. 96, pp. 226-243, 2008.

[24] S. Lu, M.J. Holst, R.E. Bank, A.D. McCulloch, and A.P. Michailova, "3-D model of synchronous calcium signaling in ventricular myocyte", *Biophys. J.*, vol. 88, pp.136A, 2005.

[25] H. Satoh, L.M. Delbridge, L A Blatter, and D M Bers, "Surface:volume relationship in cardiac myocytes studied with confocal microscopy and membrane capacitance measurements: species-dependence and developmental effects", *Biophys. J.*, vol. 70(3), pp.1494-14504, 1996.

[26] E. Page, "Quantitative ultrastructural analysis in cardiac membrane physiology", *Am. J. Physiol.*, vol. 235, pp. C146-C158, 1978.

[27] A. Michailova, F. DelPrincipe, M. Egger, and E. Niggli, "Spatiotemporal features of Ca^{2+} signaling, buffering and diffusion in atrial myocytes with inhibited sarcoplasmic reticulum", *Biophys. J.*, vol. 83, pp. 3134-3151, 2002.

[28] A. Zahradnikova, Z. Kubalova, J. Pavelková, S. Györke, and I. Zahradník, "Activation of calcium release assessed by calcium release-induced inactivation of calcium current in rat cardiac myocytes." *Am. J. Physiol. Cell. Physiol.*, vol. 286(2), pp. C330-C341, 2004.

[29] R. Hinch, J.L. Greenstein, A.J. Tanskanen, L. Xu, and R.L. Winslow, "A simplified local control model of calcium induced calcium release in cardiac ventricular myocytes", *Biophys. J.*, vol. 87, pp. 3723-3736, 2004.

[30] J. Schöberl, NETGEN - automatic mesh generator, http://www.hpfem.jku.at/netgen/.

[31] B.S. Kirk, J.W. Peterson, R. Stogner, S. Petersen The libMesh library.

[32] S. Balay, K. Bushelman, V. Eijkhout, W.D. Gropp, D. Kaushik, M.G. Knepley, L.C. McInnes, B.F. Smith, and H. Zhang, "PETSc user's manual," Argonne National Laboratory, Tech. Rep. ANL-95/11, 2004.

[33] J. Sundnes, G.T. Lines, and A. Tveito, "Efficient solution of ordinary differential equations modeling electrical activity in cardiac cells", *Math. Biosci.*, vol. 172(2), pp. 55-72, 2001.

[34] Ortega, F. The General Mesh Viewer, http://www-xdiv.lanl.gov/XCM/gmv/GMVHome.html.

[35] D.M. Bers, W. H. Barry, and S. Despa, "Intracellular Na^+ regulation in cardiac myocytes". *Cardiovasc. Res.*, vol. 57, pp.897-912, 2003.

[36] C.J. Grantham and M.B. Cannell, "Ca^{2+} influx during the cardiac action potential in guinea pig ventricular myocytes", *Circ. Res.*, vol. 79, pp. 194-200, 1996.

[37] Z. Zhou and E. Neher, "Mobile and immobile calcium buffers in bovine adrenal chromaffin cells". *J. Physiol.*, vol. 469, pp.245-273, 1993.

[38] F.B. Sachse, E. Savio-Galimberti, J.I. Goldhaber, and J.H.B. Bridge, "Sub-micrometer anatomical models of the sarcolemma of cardiac myocytes based on confocal imaging", *Pacific Symposium Biocomputing*, vol. 13, pp. 390-401, 2008.

[39] W.E. Louch, V. Bito, F.R. Heinzel, R. Macianskiene, J. Vanhaecke, W. Flameng, K. Mubagwa, and K.R. Sipido, "Reduced synchrony of Ca^{2+} release with loss of T-tubules-a comparison to Ca^{2+} release in human failing cardiomyocytes", *Cardiovasc. Res.*, vol 62, pp. 63-73, 2004.

Figure Legends

Fig. 1. Panel A: Schematic drawing of the model geometry showing the single t-tubule and its surrounding half-sarcomeres. The top surface of the cube is the surface membrane for the model compartment. Panel B: A diagram illustrating Ca^{2+} entrance and extrusion along the t-tubule and surface membrane and Ca^{2+} buffering and diffusion inside the cell when the SR release and uptake are inhibited.

Fig. 2. Panel A: The distribution of L-type Ca^{2+} current was computed (*dashed line*) by multiplying the experimentally measured cluster density and fluorescent intensity plots (*solid line*), [8], [16]. Panel B: The L-type Ca^{2+} current density was fitted and plotted (*dashed line*) using shape preserving function of the data reported in rats with SR blocked (*solid line*), [28].

Fig. 3. Panel A: The finite element software package contained four components with data flowing from top to bottom. Panel B: Composite view of the subdomain–to-processor assignment used to partition the mesh on 10 processors.

Fig. 4. Model predictions in the presence of 100 μM Fluo-3. The voltage-clamp protocol and the whole-cell L-type Ca^{2+} current used in this set of simulations are shown in panels A-B. Predicted global Na^+/Ca^{2+}, Ca^{2+} pump and leak currents and global Ca^{2+} transient

when Ca^{2+} was uniformly distributed inside the cell are shown in panels C-F. Calcium concentrations visualized as line-scan images in transverse cell direction are shown in panels G-I. Panels J-L show the local Ca^{2+} transients taken at three featured spots along the scanning line (0.17μm – *blue lines*, 3.09μm – *green lines*, 6.65μm – *red lines*). In panels G and J the L-type Ca^{2+} current density followed heterogeneous distribution in the t-tubule that was 6 times higher than in surface membrane and increased 1.7 times along the length of t-tubule as shown in Fig.2A. In panels H and K the L-type Ca^{2+} current density was uniform along the t-tubule and 6 times higher than in surface membrane. In panels I and L the L-type Ca^{2+} current density was homogeneous throughout the cell surface. In this numerical experiment Na^+/Ca^{2+} current density was 3 times higher in the t-tubule membrane, Ca^{2+} pump was located only on the surface membrane, and Ca^{2+} leak was distributed homogeneously via the sarcolemma. Panel M illustrates local Ca^{2+} time-courses with re-plot from experimental data [8]. The re-plots were taken along the scanned line at 0μm (*blue*), 3.96μm (*green*) and 7.57μm (*red*) from the near surface location. Panels J and M demonstrate that model predictions are in agreement with the experiment only when Ca^{2+} influx and efflux pathways were distributed heterogeneously. The scanned lines (*model and experiment*) were located at 200nm from the surface of the t-tubule (see *red line* in Fig. 5A).

Fig. 5. Predicted 3-D Ca^{2+} concentration distributions (*computed from the line-scan images in* Figs. 4G-I) at Ca^{2+} peak of 68 ms are shown in panels A-C. In panel D the spatial profiles at Ca^{2+} peak along the scanning line (*200nm from the surface of the t-tubule*) are compared: *gray line* - Ca^{2+} pathways heterogeneously distributed on the t-

tubule and surface membrane (see panel A); *violet line* - Ca^{2+} pathways uniformly distributed on the t-tubule (see panel B); *pink line* - Ca^{2+} pathways uniformly distributed via the sarcolemma (see panel C). Local Ca^{2+} concentration profiles at two different line-scan positions (0 nm - *solid lines, 875 nm - '+' plots*) are superimposed in panels E-G. Along the t-tubule the three featured spots were (0μm - *blue lines*, 3.48 μm - *green lines*, 6.76 μm - *red lines*) and in the cell interior (0μm - *blue lines*, 1.63 μm - *green lines*, 6.51 μm - *red lines*). In panels E-G the Ca^{2+} pathways were distributed heterogeneously or uniformly in the t-tubule membrane (as in panels A and B) or evenly along the cell surface (as in panel C).

Fig. 6. Model predictions in the absence of Fluo-3 with heterogeneous distribution of Ca^{2+} pathways via the cell membrane. Panels A and B show the voltage-clamp protocol and whole-cell L-type Ca^{2+} current used in this set of simulations. The predicted global Na^+/Ca^{2+}, Ca^{2+} pump and leak currents are presented in panels C-E. The global Ca^{2+} transient and Ca^{2+} concentrations visualized as line-scan image in the transverse cell direction are shown in panels F and G. In panel H the local Ca^{2+} transients at three spots along the scanning line are superimposed (*blue line* - 0.17μm, *green line* - 3.09μm, *red line* - 6.65μm). Panel K shows 3-D view of Ca^{2+} concentration distribution at Ca^{2+} peak (~68 ms). Scanning line in panels G-H and K was located at 200nm from the surface of the t-tubule. The local Ca^{2+} concentration profiles at two different line-scan positions (0 nm - *solid lines,* 875 nm - '+' plots) are superimposed in panel I. Panel J is an expanded view of panel I. On the t-tubule membrane and in the cell interior the featured spots were chosen to be the same as in Fig. 5E.

Fig. 7. T-tubular network complexity in adult mammalian ventricular myoyctes. Cardiac sarcolemma including t-tubules was stained with Alexa-488-conjugated wheat germ agglutinin (WGA) in 80 μm vivratome sections of adult mouse ventricular myocardium and visualized using a 2-photon microscopy (Radians 2000, BioRad, objective: 60x oil, NA=1.40, ex 800 nm, em 508-558, 59 nm/pixel). T-tubules invaginated from the surface membrane are shown to develop extensively branching in the middle of myocyte. Surface membrane (*blue arrows*), t-tubules (*white arrowheads*), nucleus (*Nuc*), bar 2 μm. The image was kindly supplied by Masahiko Hoshijima and Takeharu Hayashi (*unpublished data*).

A — Surface membrane, T-tubule, Cytoplasm

B — Ca^{2+}, NCX, LCC, Pump, Leak, SR, Fluo-3, ATP, CAL, TN

Figure 1

Figure 2

A

Mesh
Generator

↓

Finite Element
Assembler

↓

Linear System
Solver

↓

Graphic
Viewer

B
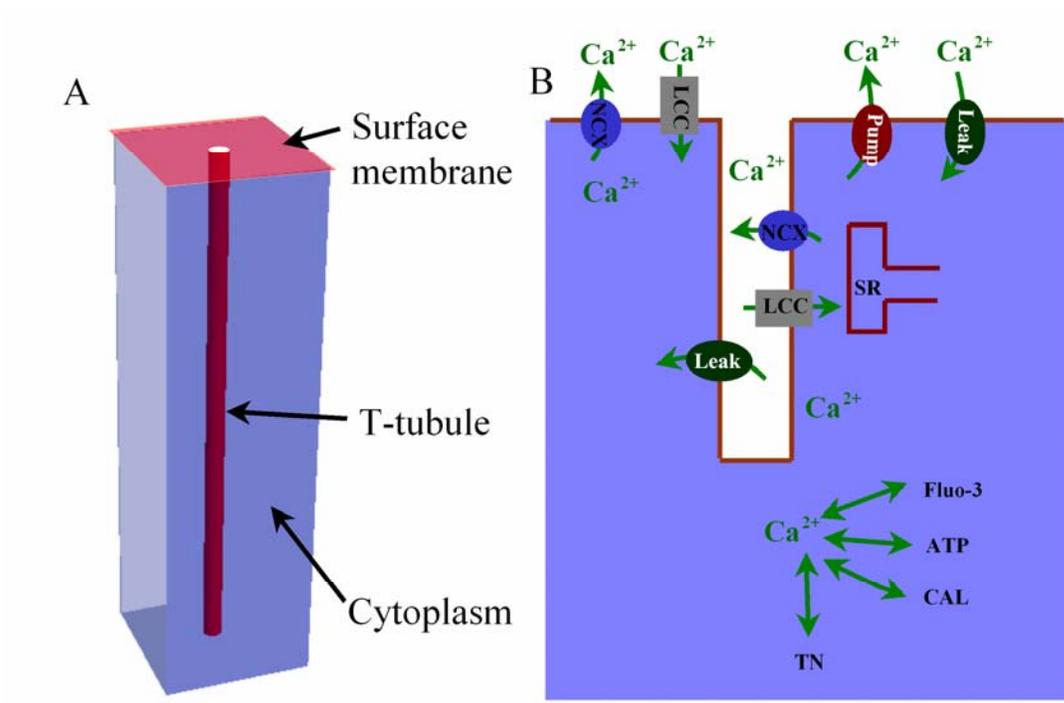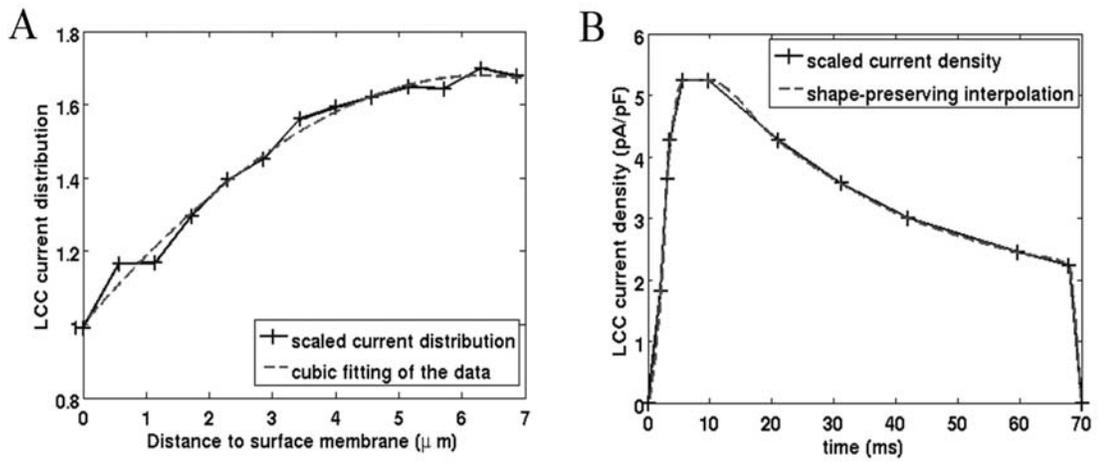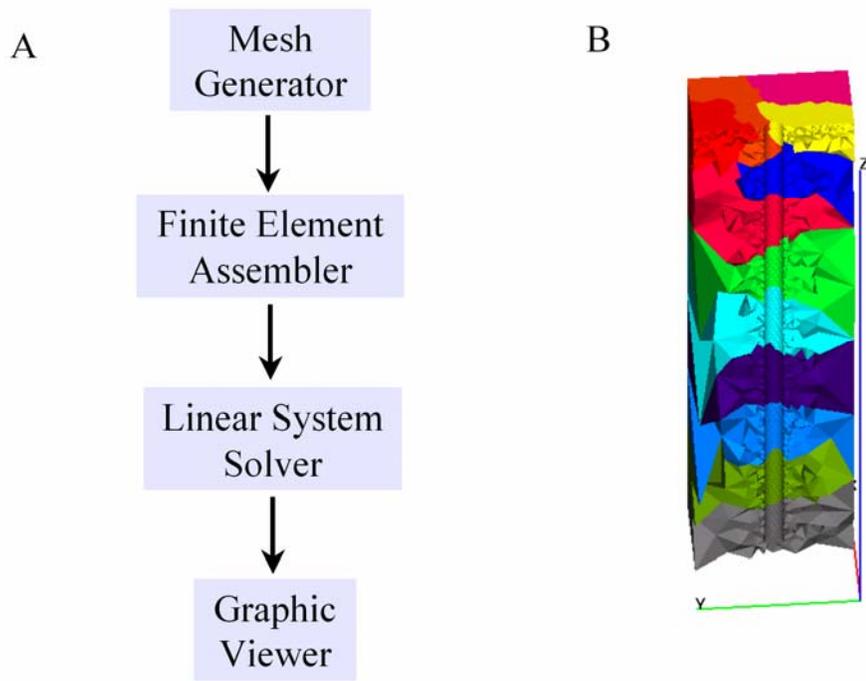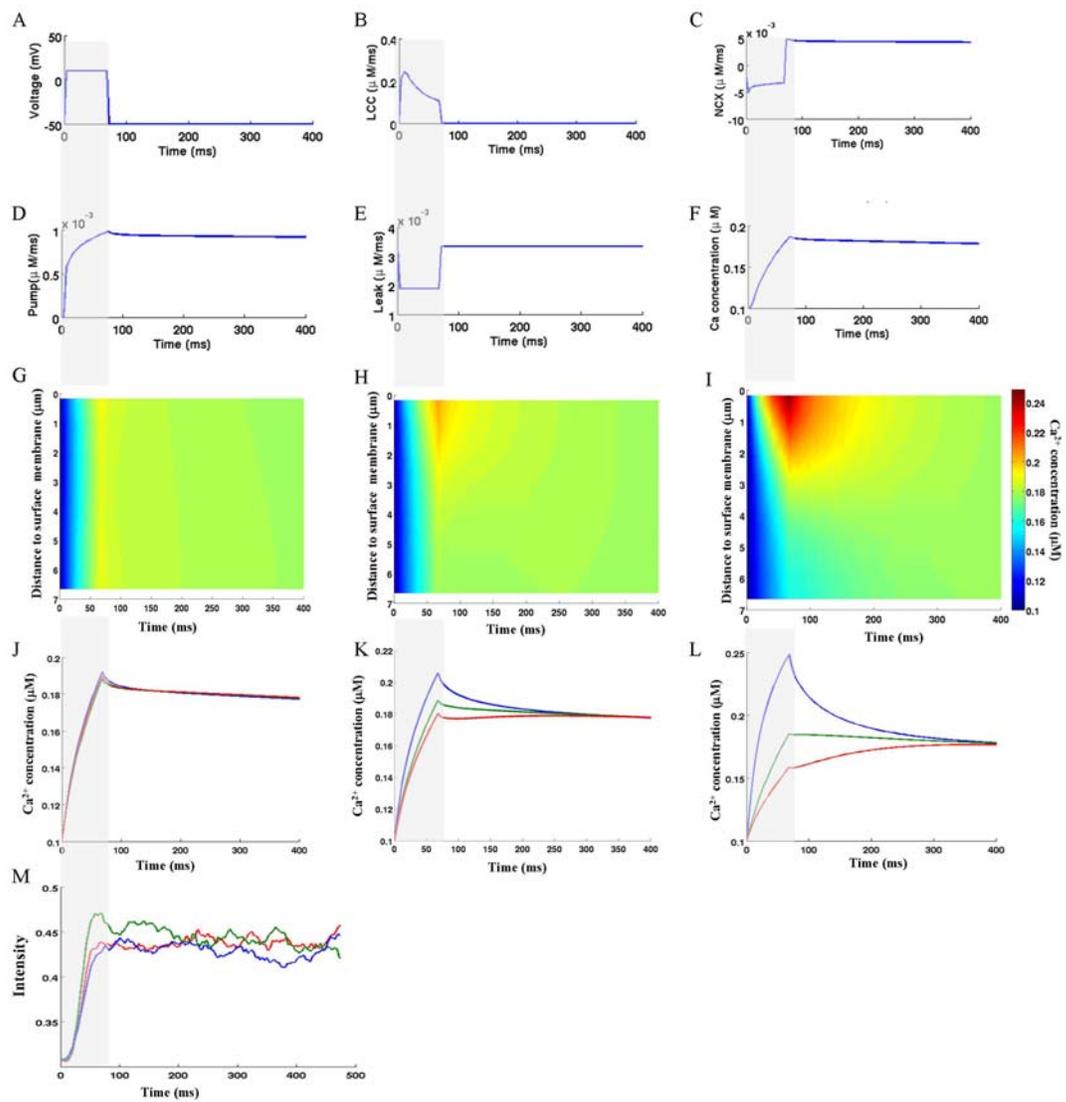
Figure 3

Figure 4

Figure 5

Figure 6

Nuc
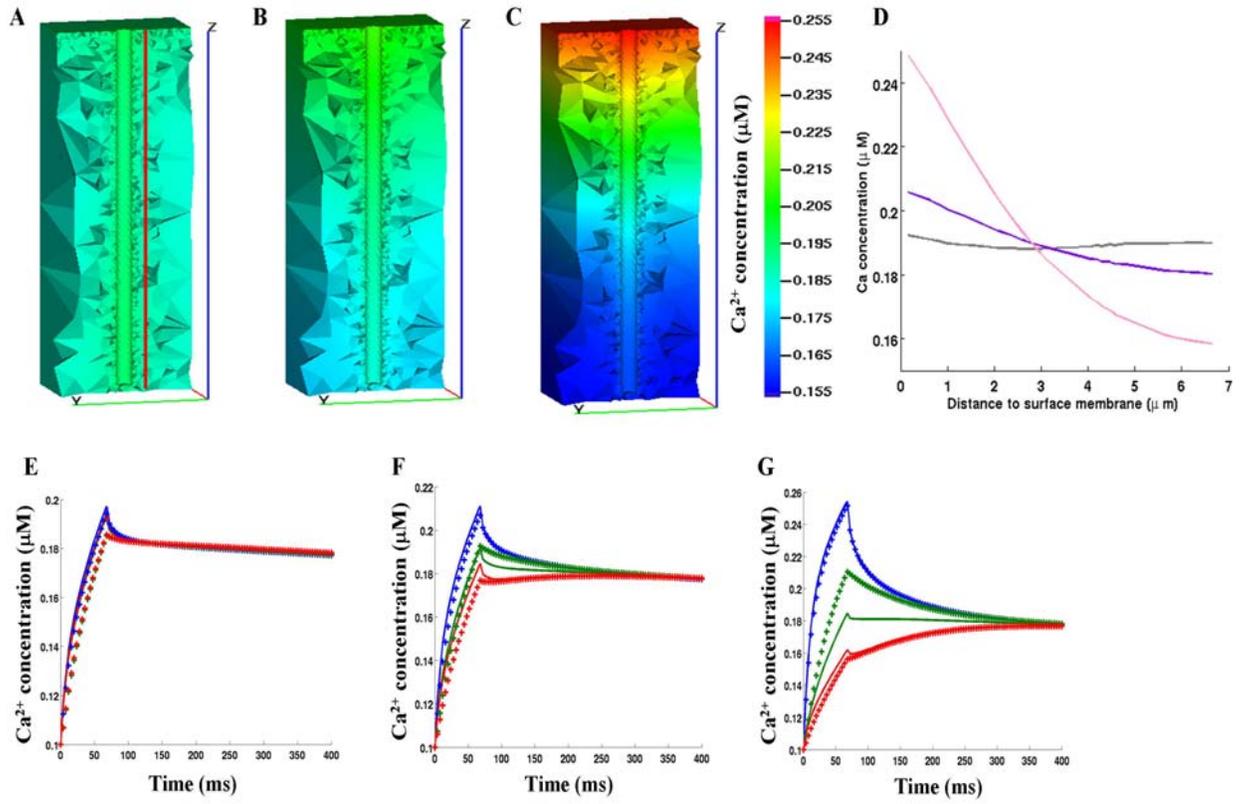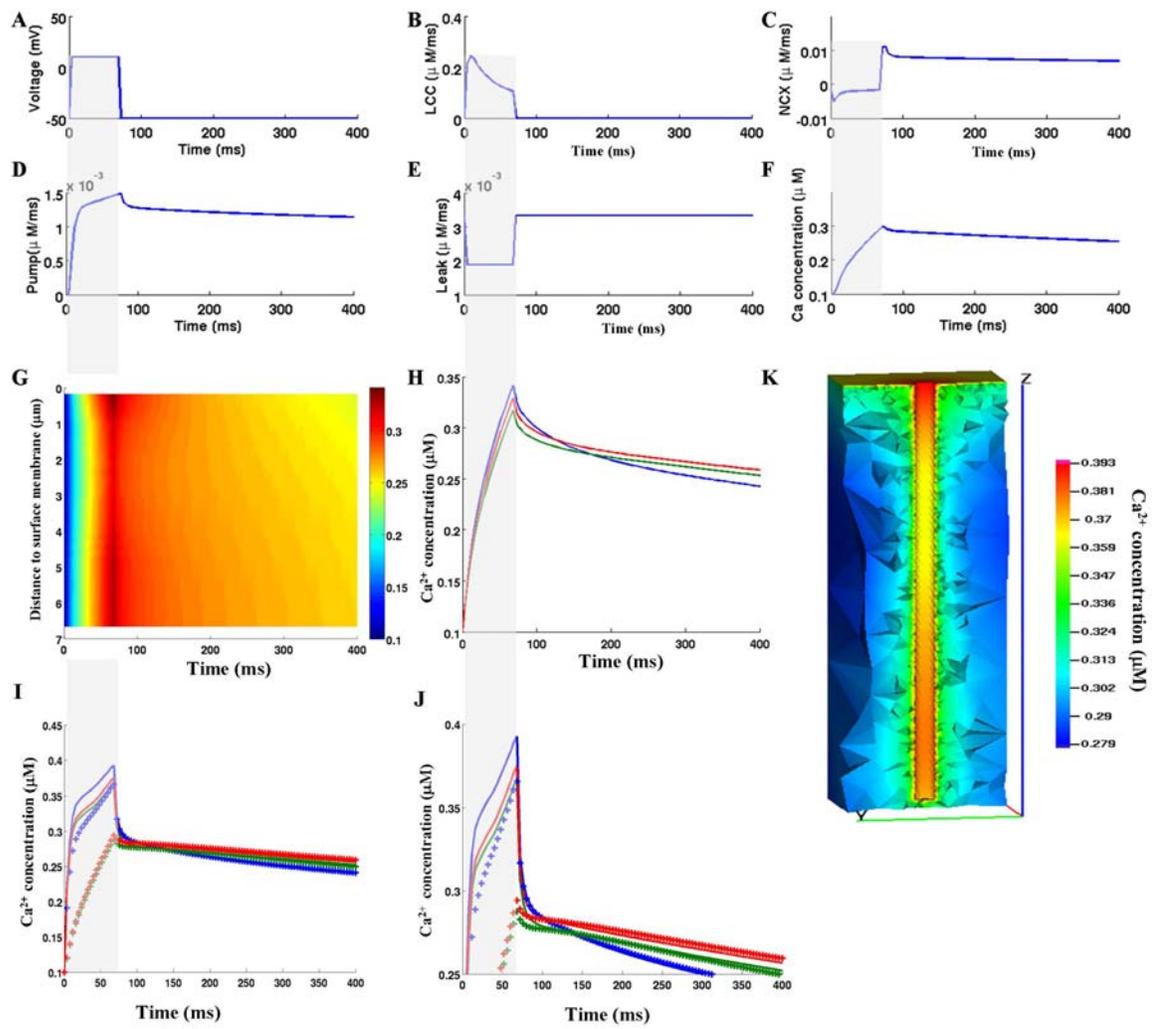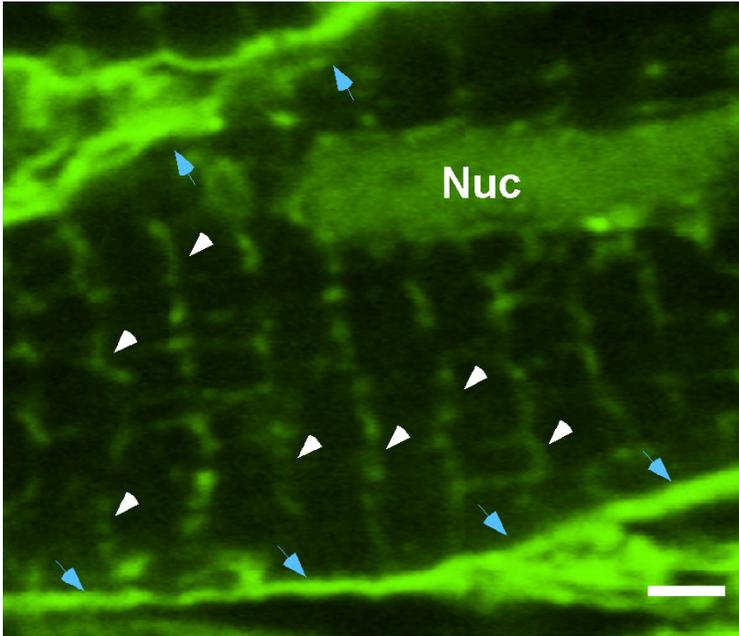
Figure 7

Table 1. Physical constants and cell geometry

Definition	Symbol	Value	Reference No.
Faraday constant	F	96.5 C mmol^{-1}	Physical constant
Temperature	T	295 K	Physical constant
Universal gas constant	R	8.314 J mol^{-1} K^{-1}	Physical constant
Cell volume	V_{cell}	36.8 pL	[1]
Cell capacitance	C_m	324 pF	[1]
Accessible volume for Ca^{2+} in the cell	V_{acc}	12.9-13.6 pL	Estimated
Compartment volume	V_{mc}	27.68 µm^3	Estimated
Compartment surface	S_{mc}	9.34 µm^2	Estimated
T-tubule geometry			
T-tubule radius	r_{t-tub}	0.125 µm	[9]
T-tubule depth	dp_{t-tub}	6.87 µm	[9]
Cubic-shaped box geometry			
Cell surface direction	d_{box-1}	2µm	[9]
Cell surface direction	d_{box-2}	2µm	[9]
Depth	dp_{box}	7µm	[9]

Table 2. The parameter values of cubic polynomial describing the L-type Ca^{2+} current distribution along the t-tubule

Symbols	C	p$_1$	p$_2$	p$_3$	p$_4$
L-type Ca^{2+} channel	0.6827	-4.1379e-4	-1.1722e-2	1.978e-1	1.0033

Table 3. Ca^{2+} and buffer reaction-diffusion parameters

Definition	Symbol	Value	Reference No.
Ca^{2+} and buffer concentrations			
Extracellular Ca^{2+} concentration	$[Ca^{2+}]_e$	1000 µM	[1]
Resting Ca^{2+} concentration	$[Ca^{2+}]_{i0}$	0.1 µM	[1]
Total Fluo-3 concentration	$[Fluo]$	100 µM	[27]
Total free ATP concentration	$[ATP]$	260 µM	[27]
Total troponin concentration	$[TN]$	70 µM	[27]
Total calmodulin concentration	$[Cal]$	24 µM	[27]
Diffusion coefficients (at 22ºC)			
Diffusion coefficient for Ca^{2+}	D_{Ca}	0.39 µm^2 ms^{-1}	[27]
Diffusion coefficient for CaFluo	D_{CaFluo}	0.1 µm^2 ms^{-1}	[27]
Diffusion coefficient for CaATP	D_{CaATP}	0.168 µm^2 ms^{-1}	[27]
Diffusion coefficient for CaCal	D_{CaCal}	0.025 µm^2 ms^{-1}	[27]
Rate coefficients (at 22ºC)			

Ca^{2+} on-rate constant for TN	k_+^{CaTN}	0.04 μM^{-1} ms^{-1}	[27]
Ca^{2+} off-rate constant for TN	k_-^{CaTN}	0.04 ms^{-1}	[27]
Ca^{2+} on-rate constant for CaATP	k_+^{CaATP}	0.225 μM^{-1} ms^{-1}	[27]
Ca^{2+} off-rate constant for CaATP	k_-^{CaATP}	45 ms^{-1}	[27]
Ca^{2+} on-rate constant for CaFluo	k_+^{CaFluo}	0.23 μM^{-1} ms^{-1}	[27]
Ca^{2+} off-rate constant for CaFluo	k_-^{CaFluo}	0.17 ms^{-1}	[27]
Ca^{2+} on-rate constant for Cal	k_+^{CaCal}	0.125 μM^{-1} ms^{-1}	[27]
Ca^{2+} off-rate constant for Cal	k_-^{CaCal}	0.2975 ms^{-1}	[27]

Table 4. Membrane Ca^{2+} fluxes parameters

Definition	Symbol	Value	Reference No.
Na$^+$/Ca^{2+} exchange current			
Extracellular Na$^+$ concentration	$[Na^+]_e$	140 mM	[1]
Resting Na$^+$ concentration	$[Na^+]_i$	10 mM	[1]
Pump rate of NCX	g_{NCX}	38.5 μM ms^{-1}	[29]
Voltage dependence of NCX control	η	0.35	[29]
Na$^+$ half saturation of NCX	$k_{m,Na}$	87.5 mM	[29]
Ca^{2+} half saturation of NCX	$k_{m,Ca}$	1380 μM	[29]
Low potential saturation factor of NCX	k_{sat}	0.1	[29]
membrane Ca^{2+} ATPase			
Maximum Ca^{2+} pump rate	g_{pCa}	0.0035μM ms^{-1}	[29]
Half saturation of Ca^{2+} pump	$k_{m,pCa}$	0.5 μM	[29]
membrane Ca^{2+} leak			
Conductance of sarcolemmal Ca^{2+} leak	g_{Cab}	1.65e-5μM mV^{-1}ms^{-1}	Estimated